



## RESEARCH ARTICLE

# Investigation of the applicability of TiO<sub>2</sub>, BiVO<sub>4</sub>, and WO<sub>3</sub> nanomaterials for advanced photocatalytic membranes used for oil-in-water emulsion separation

Erika Nascimben Santos<sup>1</sup> | Áron Ágoston<sup>1</sup> | Szabolcs Kertész<sup>1</sup> |  
Cecilia Hodúr<sup>1,2</sup> | Zsuzsanna László<sup>1</sup> | Zsolt Pap<sup>2</sup> | Zsolt Kása<sup>2</sup> |  
Tünde Alapi<sup>3</sup> | S.A. Gokula Krishnan<sup>4</sup> | Gangasalam Arthanareeswaran<sup>4</sup> |  
Klara Hernadi<sup>5</sup> | Gábor Veréb<sup>1</sup>

<sup>1</sup>Institute of Process Engineering, Faculty of Engineering, University of Szeged, Szeged, Hungary

<sup>2</sup>Institute of Environmental Science and Technology, University of Szeged, Szeged, Hungary

<sup>3</sup>Department of Inorganic and Analytical Chemistry, Institute of Chemistry, University of Szeged, Szeged, Hungary

<sup>4</sup>Department of Chemical Engineering, National Institute of Technology, Membrane Research Laboratory, Tiruchirappalli, India

<sup>5</sup>Department of Applied and Environmental Chemistry, Institute of Chemistry, University of Szeged, Szeged, Hungary

## Correspondence

Gábor Veréb, Institute of Process Engineering, Faculty of Engineering, University of Szeged, HU-6725, Moszkvai Blvd. 9., Szeged, Hungary.  
Email: verebg@mk.u-szeged.hu

## Funding information

Hungarian Ministry of Human Capacities, Grant/Award Number: UNKP-18-4-SZTE-78; University of Szeged Open Access Fund, Grant/Award Number: 4541; University of Szeged, Grant/Award Number: 4541; Hungarian Academy of Sciences, Grant/Award Number: János Bolyai Research Scholarship; Stipendium Hungaricum; Ministry of Science and Technology of the Government of India,

## Abstract

In the present study, a commercial TiO<sub>2</sub>, several BiVO<sub>4</sub> photocatalysts, a WO<sub>3</sub> nanomaterial, and their composites were used to prepare photocatalytic polyvinylidene fluoride (PVDF) ultrafilter membranes. Their photocatalytic activities and the effects of coatings on the filtration of oil-in-water emulsion (crude oil; c<sub>oil</sub> = 100 mg L<sup>-1</sup>) were investigated. Fluxes, filtration resistances, purification efficiencies, and fouling resistance abilities—like flux decay ratios (FDRs) and flux recovery ratios (FRRs)—were compared. The solar light-induced photocatalytic decomposition of the foulants was also investigated. WO<sub>3</sub> was used as a composite component to suppress the electron–hole recombination with the goal of achieving higher photocatalytic activity, but the presence of WO<sub>3</sub> was not beneficial concerning the filtration properties. However, the application of TiO<sub>2</sub>, one of the investigated BiVO<sub>4</sub> photocatalysts, and their composites was also beneficial. In the case of the neat membrane, only 87 L m<sup>-2</sup> h<sup>-1</sup> flux was measured, whereas with the most beneficial BiVO<sub>4</sub> coating, 464 L m<sup>-2</sup> h<sup>-1</sup> flux was achieved. Pure BiVO<sub>4</sub> coating was more beneficial in terms of filtration properties, whereas pure TiO<sub>2</sub> coating proved to be more beneficial concerning the photocatalytic regeneration of the membrane. The TiO<sub>2</sub>(80%)/BiVO<sub>4</sub>(20%) composite was estimated to be the most beneficial combination taking into account both the aspects of photocatalytic activity and filtration properties.

## KEYWORDS

bismuth vanadate, oil emulsion, photocatalytic membrane, solar irradiation, titanium dioxide, tungsten trioxide

This is an open access article under the terms of the Creative Commons Attribution License, which permits use, distribution and reproduction in any medium, provided the original work is properly cited.

© 2020 The Authors. Asia-Pacific Journal of Chemical Engineering published by Curtin University and John Wiley & Sons Ltd

Grant/Award Number:  
DST/INT/HUN/P17/2017; Hungarian  
State and the European Union, Grant/  
Award Number: EFOP-  
3.6.2-16-2017-00010; Hungarian Science  
and Research Foundation, Grant/Award  
Number: 2017-2.3.7-TÉT-IN-2017-00016

## 1 | INTRODUCTION

Increasing amounts of oily wastewaters are produced all over the world by several industrial activities (such as oil refining and metal and food industries<sup>1,2</sup>) and also during the continuous cleaning of the increasing amount of registered vehicles—it is estimated to be 2 billion until 2035.<sup>3,4</sup> These wastewaters contain several contaminations that has been proven to pose serious risks to both the natural environment and human health.<sup>5–7</sup> Hydrocarbons in particular can be harmful to living organisms because of coating and poisoning.<sup>8,9</sup> Oil contaminations can reduce the bacterial activity of soils and also the plant growth by affecting the root elongation and germination.<sup>10,11</sup> Concerning animals and human beings, some oil contaminations can damage the DNA and produce genotoxic, carcinogenic, and mutagenic effects; moreover, many of these compounds are persistent and can accumulate through the food chain.<sup>12–14</sup>

Because of these harmful effects and the growing production of these kinds of wastewaters, more stringent emission limits have to be imposed to protect the environment and the health of humanity. Therefore, the development of effective treatment methods of oily wastewaters is of great interest.<sup>15,16</sup> To comply with the stringent emission limits, conventional techniques—such as skimming,<sup>17</sup> sand filtration,<sup>18</sup> centrifugation,<sup>19</sup> flotation,<sup>20</sup> adsorption,<sup>5</sup> or chemical destabilization<sup>21,22</sup>—must be augmented with advanced method(s) such as membrane filtration, which can eliminate the usually remaining microsized and nanosized oil droplets.<sup>23–26</sup>

Membrane filtration has numerous advantages, like high purification efficiency, facile operation, easy integration, and the absence of chemical additives.<sup>26,27</sup> However, for its economic utilization, the mitigation of membrane fouling needs to be solved, especially in the case of oily wastewaters, because the formation of hydrophobic layer results in significant flux reduction, which reduces the productivity and life span of the membrane and increases the energy consumption and the cost of the treatment.<sup>25</sup> A promising way to solve the flux reduction is to minimize the interaction between the oily foulants and membrane surface by improving the membrane's hydrophilicity.<sup>28,29</sup> Different nanomaterials can be used for this purpose, thus achieving higher flux and even higher rejection rates

compared with conventional membranes.<sup>30–32</sup> Titanium dioxide (TiO<sub>2</sub>) nanoparticles proved to be useful in enhancing the membrane's hydrophilicity—therefore achieving higher fluxes—during the filtration of oily wastewaters.<sup>33–39</sup> Moreover, TiO<sub>2</sub>—as a photocatalytic semiconductor—also enables the photocatalytic degradation of organic foulants without the addition of chemicals, only by activating them with simple UV, visible, or solar light irradiation,<sup>40–42</sup> thus generating charge carriers (electrons [e<sup>-</sup>] and holes [h<sup>+</sup>]) and highly oxidative radicals (such as hydroxyl radical), which can decompose organic contaminants.

Therefore, photocatalytic membrane reactors (PMRs)—equipped with photocatalyst-modified membrane surfaces—are able to eliminate organic fouling contaminants and to recover the flux via an efficient and chemical-free way that is based on the photocatalytically generated oxidative species.<sup>40,41,43,44</sup> Immobilization of photocatalytic nanoparticles can be carried out by physical deposition,<sup>37,45,46</sup> cross-linking,<sup>47</sup> in situ precipitation,<sup>33</sup> dip coating,<sup>48</sup> grafting,<sup>35</sup> blending,<sup>34,39,43,49</sup> and so forth. There are numerous studies in the literature that proved the beneficial properties of these photocatalytic membranes—such as lower filtration resistances, reduced fouling, increased flux, higher separation efficiency, advanced flux recovery, and self-cleaning ability—during the filtration of wastewaters containing dyes,<sup>46,47</sup> oils,<sup>33–38,45–49</sup> or other hydrocarbons.<sup>34,35,46</sup>

TiO<sub>2</sub> is probably the most investigated photocatalyst because of its numerous beneficial properties—such as low cost, chemical stability, relatively high photocatalytic activity, and easy preparation<sup>50</sup>—but it is not free from drawbacks, because the significant electron/hole (e<sup>-</sup>/h<sup>+</sup>) recombination limits the photocatalytic activity, and pure TiO<sub>2</sub> can be activated mainly by UV photons. Therefore, many researchers seek to suppress e<sup>-</sup>/h<sup>+</sup> recombination more effectively and to reduce the semiconductors' band gap values, thus reaching higher solar light-induced excitability. These efforts are also important for the development of photocatalytic membrane surfaces. For the suppression of e<sup>-</sup>/h<sup>+</sup> recombination, for example, carbon nanotubes (CNTs) can be used as a composite component because of their high conductivity<sup>51</sup>; moreover, the presence of CNTs on the membrane surface also proved to be beneficial in the case of oil-in-water (o/w) emulsion separation.<sup>38</sup> Utilization of tungsten trioxide (WO<sub>3</sub>) as a composite component can also be beneficial to suppress e<sup>-</sup>/h<sup>+</sup>

recombination,<sup>48,52,53</sup> whereas bismuth vanadate ( $\text{BiVO}_4$ )—a well-known visible light active photocatalyst<sup>54–60</sup>—is also promising for use for membrane surface modification to reach higher solar light-induced excitability.

On the basis of these considerations—which are summarized in Figure 1—in the present study, commercial  $\text{TiO}_2$ ,  $\text{WO}_3$ , five different home-made  $\text{BiVO}_4$  photocatalyst, and their composites were immobilized onto polyvinylidene fluoride (PVDF) ultrafilter (UF) membranes. Their photocatalytic activities were investigated in detail, using both visible and UV light excitations. The filtration of o/w emulsions was also investigated using the nanomaterial-modified membranes: achievable fluxes, filtration resistances, and characteristics concerning the fouling resistant ability—like flux decay ratios (FDRs) and flux recovery ratios (FRRs)—were compared in detail. Moreover, the solar light-induced photocatalytic decomposition of the foulants was also investigated.

## 2 | MATERIAL AND METHODS

### 2.1 | Synthesis of different $\text{BiVO}_4$ samples

For the present study, five different  $\text{BiVO}_4$  photocatalysts (named as  $\text{BiVO}_4$ -I-V) were synthesized by hydrothermal methods. The  $\text{BiVO}_4$ -I photocatalyst was produced by our recently optimized synthesis method: 2.5-mmol  $\text{Bi}(\text{NO}_3)_3 \cdot 5\text{H}_2\text{O}$  (Alfa Aesar,  $\geq 98\%$ , ACS) was dissolved in 55.7 ml of 2-M nitric acid (Merck Millipore, 69%, ACS reagent), and 2.5-mmol  $\text{NaVO}_3$  (Sigma Aldrich,  $\geq 98\%$  [RT]) was dissolved in 55.7 ml of distilled water. The two

solutions were stirred continuously for 20 min at room temperature, and then the  $\text{NaVO}_3$  solution was added dropwise to the other solution under vigorous stirring. After the appearance of a yellow precipitate, the solution was additionally stirred for 30 min, and then the pH value was adjusted to 5 by the dropwise addition of 10- and 2-M  $\text{NaOH}$  (Sigma-Aldrich, 100%, puriss) solution. One hundred twenty milliliters of the resulting solution was transferred into a 150-ml Teflon-lined stainless steel autoclave, and the hydrothermal treatment was carried out at  $180^\circ\text{C}$  for 15 h. The products were washed by centrifugation (applying 4,400 rpm stirring speed) three times with ethanol as purifying solvent and three times with Milli-Q water, and then the synthesized  $\text{BiVO}_4$  nanoparticles were dried at  $60^\circ\text{C}$  for 24 h, and the powder was ground in an agate mortar.

During the synthesis of  $\text{BiVO}_4$ -II and III photocatalysts,  $\text{NH}_4\text{VO}_3$  (Sigma Aldrich,  $\geq 99\%$ , ACS reagent) was used as vanadium-containing precursor (in the same concentration: 2.5 mmol; same volume: 55.7 ml), and the pH value was adjusted to 5 by the addition of 15 wt.%  $\text{NH}_4\text{OH}$  (Sigma-Aldrich, 25%, reagent grade) solution to avoid  $\text{Na}^+$  addition. Fluoride ions were used—by adding  $\text{NH}_4\text{F}$  (VWR,  $\geq 98\%$ , ACS reagent) to the solution—to modify the surface, because by the fluorination of  $\text{BiVO}_4$  crystals, the direct oxidation of the adsorbed molecules by the holes can be intensified, as it was described by Liu et al.<sup>59</sup> In the case of  $\text{BiVO}_4$ -II, a  $\text{Bi}^{3+}:\text{F}^- = 1:1$  molar ratio was used, whereas in the case of  $\text{BiVO}_4$ -III, this ratio was 2:1. The synthesized bismuth vanadates were purified with centrifugation, and then they were dried and ground the same as before.



**FIGURE 1** Schematic figure about the mechanism of the photocatalytic decomposition of oily contaminants on the membrane surfaces and about the required beneficial properties of novel photocatalysts

The BiVO<sub>4</sub>-IV and BiVO<sub>4</sub>-V samples were synthesized by following the methods of Jiang et al.,<sup>60</sup> which can be used to produce porous BiVO<sub>4</sub>. This property can potentially be beneficial when the material is used for the surface modification of membranes. Twenty millimoles of Bi(NO<sub>3</sub>)<sub>3</sub>·5H<sub>2</sub>O was dissolved in 100 ml of 2-M nitric acid (Merck Millipore, 69%, ACS reagent), and Pluronic P123 surfactant (BASF) was added in a calculated amount, resulting in Bi<sup>3+</sup>:P123 = 1:0.034 molar ratio. Then, 20 mmol of NH<sub>4</sub>VO<sub>3</sub> was added dropwise to the solution, and finally, the pH value was adjusted to 3 with NH<sub>4</sub>OH (Sigma-Aldrich, 25%, reag. Ph. Eur.). The hydrothermal synthesis was carried out at 80°C (BiVO<sub>4</sub>-IV) and at 100°C (BiVO<sub>4</sub>-V) for 6 h. The synthesized bismuth vanadates were purified with the previously detailed centrifugation procedure, and then it was dried and ground, the same as before. Then, the yellow powders were calcined in air at 400°C in a tube furnace (Thermolyne 21100; heat-up rate was 1°C min<sup>-1</sup>) for 4 h.

## 2.2 | Characterization of the BiVO<sub>4</sub> photocatalysts

X-ray diffraction (XRD) measurements were applied to identify the crystalline phases of the samples. The XRD patterns were recorded using a Rigaku MiniFlex II diffractometer with Cu-K<sub>α</sub> radiation ( $\lambda = 0.15406$  nm, 30 kV, 15 mA), equipped with a graphite monochromator. The XRD measurements were recorded from 10° to 65° (2 $\theta$ ). The scanning speed was 3° min<sup>-1</sup>. The average size of the crystals was calculated using the Scherrer equation.<sup>61</sup>

The morphology of the particles was analyzed by a Hitachi S-4700 Type II scanning electron microscope (SEM). The applied accelerating voltage was 10 kV. The samples were attached to an adhesive carbon tape, which was fixed to an aluminum sample holder.

The diffuse reflectance (DR) spectra of the samples ( $\lambda = 250$ –800 nm) were measured using a JASCO-V650 UV-Vis spectrophotometer equipped with an integration sphere (ILV-724). To obtain the band gap energies, the reflectance data were converted to F(R) values according to the Kubelka–Munk theory.<sup>62</sup> The band gaps were obtained from the plot of (F(R)E)<sup>1/2</sup> versus energy of the incident light.

## 2.3 | Production of nanomaterial-modified membranes

Multicomponent nanocomposites—containing homemade BiVO<sub>4</sub>, commercial TiO<sub>2</sub> (Aeroxide P25; Evonik

Industries), and WO<sub>3</sub> (Sigma-Aldrich, puriss)—were prepared by grinding them together in calculated amounts in an agate mortar for 15 min.

Forty milligrams of the given nanomaterial or nanocomposite was suspended in 100 ml of 2-propanol (Molar Chemicals Ltd., analytical grade) followed by 2 min of ultrasonic homogenization (Hielscher UP200S) at 25°C (maximal amplitude and cycle were applied). The homogenized nanoparticles were immobilized onto the surface of a PVDF UF membrane (New Logic Research Inc., MWCO: 100 kDa; 1.0 mg cm<sup>-2</sup> catalyst coverage) by physical deposition: the suspension was filtered through the membrane in a batch-stirred membrane reactor (Millipore, XFUF07601), applying high (0.3 MPa) transmembrane pressure, and then the membranes were dried in air at room temperature.

## 2.4 | Photocatalytic activity measurements

The photocatalytic activities of the different BiVO<sub>4</sub> samples were compared by the photocatalytic decomposition of methylene blue solutions in a double-walled, thermostated (25°C) glass photoreactor, which was surrounded with a LED strip (5050 SMD type;  $l = 1$  m; cool white; 60 pcs of LEDs; 14.4 W; 1,170 lm), which emits only visible light (Figure 2). One hundred milligrams of the given photocatalyst was suspended in 100 ml of distilled water with ultrasonic homogenization (Hielscher UP200S; 25°C; 2 min), and then methylene blue was added to the suspension ( $c = 1.0 \times 10^{-5}$  mol L<sup>-1</sup>). During the photocatalytic experiments, the suspension was stirred intensively with a magnetic stirrer. After taking the samples, they were centrifuged (Thermo Scientific Megafuge 16R; 13,000 rpm; 2 min), filtered (0.25  $\mu$ m), and finally analyzed with a spectrophotometer (Biochrom Biowave II+) by measuring the absorbance at  $\lambda = 661$  nm.

The photocatalytic activities of the different TiO<sub>2</sub>/WO<sub>3</sub> composite-coated membranes were determined by the photocatalytic decomposition of methyl orange ( $c = 1.0 \times 10^{-5}$  mol L<sup>-1</sup>,  $V = 100$  ml) in a modified Millipore (XFUF07601) membrane reactor equipped with different light tubes (Lightech; 10 W; UV<sub>365nm</sub> or Vis) and a magnetic stirrer (Figure 3).

## 2.5 | Production of oil-in-water emulsions

The o/w emulsions ( $c_{\text{oil}} = 100$  mg L<sup>-1</sup>) contained crude oil (provided by a South Hungarian oil production company), and the oil droplets had a diameter of 50–1,500 nm



**FIGURE 2** (a) Schematic figure and (b) photograph of the photoreactor used to compare the visible light excitability of the bismuth vanadate photocatalysts

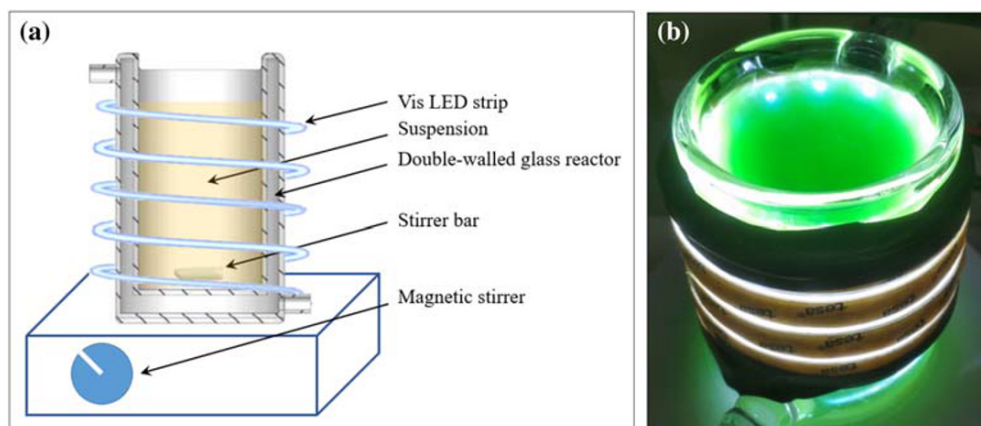
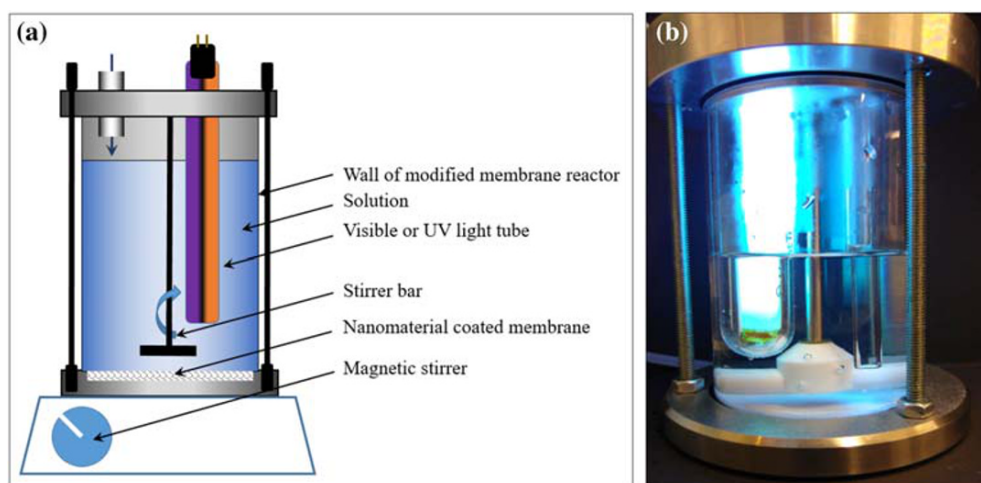


**FIGURE 3** (a) Schematic figure and (b) photograph of the photoreactor which was used for the comparison of the photocatalytic activities of different  $\text{TiO}_2/\text{WO}_3$  nanocomposite-covered membranes



with an average droplet size of  $\sim 500$  nm (determined by dynamic light scattering measurements). Their preparation was carried out in two steps: an intensive mixing (Skil F0151415AC; 35,000 rpm), which was followed by a 10-min-long ultrasonic homogenization (Hielscher UP200S) at 24 kHz frequency (using maximal amplitude and cycle) providing constant  $25^\circ\text{C}$  temperature by circulating water in the thermostating jacket of the double-walled glass reactor.

## 2.6 | Membrane filtration experiments

The filtration experiments with the o/w emulsions were carried out in a batch-stirred membrane reactor (Millipore XFUF07601, USA), which was equipped with the given commercial or nanomaterial-modified PVDF UF membrane (New Logic Research Inc., MWCO: 100 kDa; 76 mm diameter; active filtration area:  $37.4\text{ cm}^2$ ), using 0.1 MPa transmembrane pressure and  $5.83\text{ s}^{-1}$  stirring speed (350 rpm). In all cases, 250-ml emulsion was added into the reactor, which was followed

by filtration until the production of 200-ml permeate (volume reduction ratio:  $\text{VRR} = 5$ ). Purification efficiencies were determined by measuring the chemical oxygen demand (COD) and the extractable oil content (TOG/TPH) of the feed and the permeate. The measurement of COD was based on a standard potassium dichromate-oxidation method, using standard test vials (Hanna Instruments). The digestions were carried out in a COD digester (Lovibond, ET 108) for 2 h at  $150^\circ\text{C}$ , and the COD values were measured with a COD photometer (Lovibond PC-CheckIt). The extractable oil content was measured with a Wilks InfraCal TOG/TPH type analyzer, using hexane as extracting solvent.

### 2.6.1 | The determination of filtration resistances

The membrane resistance ( $R_M$ ) was calculated as

$$R_M = \frac{\Delta p}{J_w \eta_w} \quad (\text{m}^{-1}), \quad (1)$$

where  $\Delta p$  is the applied transmembrane pressure (Pa),  $J_W$  is the water flux of the clean membrane ( $\text{m}^3 \text{m}^{-2} \text{s}^{-1}$ ), and  $\eta_W$  is the viscosity of the water (Pa s).

The irreversible resistance ( $R_{\text{Irrev}}$ ) was determined by remeasuring the water flux on the used membrane after the filtration, followed by a purification step (intensive rinsing with distilled water):

$$R_{\text{Irrev}} = \frac{\Delta p}{J_{WA} \eta_W} - R_M \quad (\text{m}^{-1}), \quad (2)$$

where  $J_{WA}$  is the water flux after the cleaning procedure.

The reversible resistance ( $R_{\text{Rev}}$ )—caused by non-attached oil layer and concentration polarization—can be calculated as

$$R_{\text{Rev}} = \frac{\Delta p}{J_c \eta_{ww}} - R_{\text{Irrev}} - R_M \quad (\text{m}^{-1}), \quad (3)$$

where  $J_c$  is the flux at the end of the filtration and  $\eta_{ww}$  is the viscosity of the emulsion.

The total resistance ( $R_T$ ) can be calculated as the sum of the previously detailed resistances:

$$R_T = R_M + R_{\text{Irrev}} + R_{\text{Rev}} \quad (\text{m}^{-1}). \quad (4)$$

To evaluate the fouling resistance of the membranes at different conditions, the FDR and FRR were also calculated:

$$\text{FDR} = \frac{J_w - J_c}{J_w} 100\%, \quad (5)$$

$$\text{FRR} = \frac{J_{WA}}{J_w} 100\%, \quad (6)$$

where  $J_w$  is the water flux of the clean membrane,  $J_c$  is the flux at the end of the filtration of the given o/w

emulsion, and  $J_{WA}$  is the water flux after the cleaning procedure.

## 2.7 | Purification of the contaminated photocatalytic membranes by solar irradiation

After the o/w emulsion separation—followed by an intensive water rinsing—the water fluxes were measured, and then the photocatalytic purification of the contaminated membranes was carried out by natural solar irradiation. Subsequently, the water fluxes were remeasured after 150 min to describe the efficiency of photocatalytic flux recovery. For this experiment, flat ceramic beakers were placed onto a multiposition magnetic stirrer. The contaminated membranes were placed to the bottom of these ceramic beakers and fixed with O rings, as it is illustrated in Figure 4. Then, narrow (26 mm) and thin (1.0 mm) glasses were placed onto the O rings to keep a 6-mm distance between the magnetic stirring bars and the membrane surfaces for the purpose of preventing damage to the nanomaterial coating and to let the solar light reach the membrane. The glasses reduced only 20% of UV-A intensity—measured by an Optix UVTEX UV dosimeter.

## 3 | RESULTS AND DISCUSSION

### 3.1 | Characterization of home-made $\text{BiVO}_4$ photocatalysts

X-ray diffractometry was used to analyze the crystal structures of the synthesized  $\text{BiVO}_4$  photocatalysts. The measured diffractograms are presented in Figure 5, which shows a series of characteristic peaks (101, 011, 121, 040, 200, 002, 211, 051, 240, 242, 202, 222, 170, 321) in all cases, which are in accordance with the

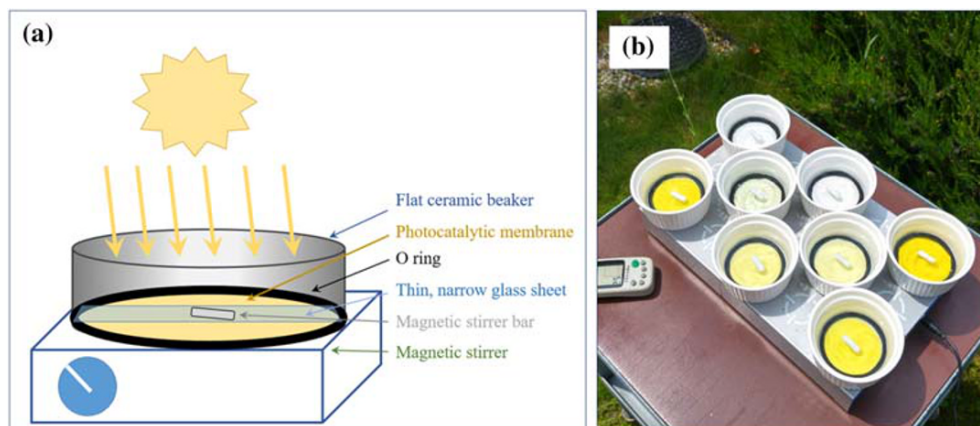
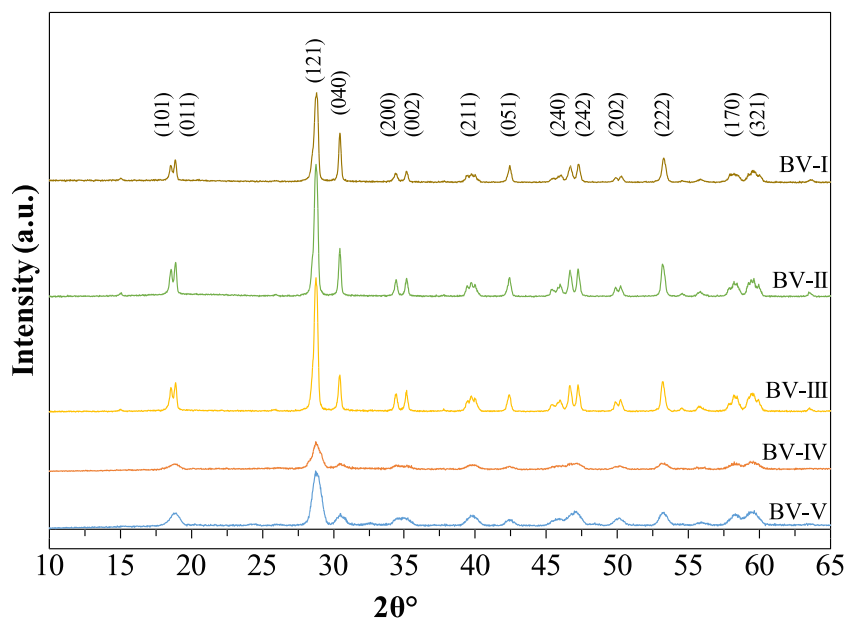


**FIGURE 4** (a) Schematic figure and (b) photograph of the experimental setup, used for the solar photocatalytic membrane cleaning experiments

**FIGURE 5** X-ray diffraction (XRD) patterns of the synthesized  $\text{BiVO}_4$  photocatalysts, showing the presence of the monoclinic crystal phase in all cases



photocatalytically active monoclinic structure (JCPDS No. 14-0688).<sup>55–57</sup>

The morphology of all the bismuth vanadate nanomaterials was characterized by SEM (Figure 6). In the case of the BV-I sample, thin and anisotropic crystallites were observed, whereas BV-II—synthesized in the presence of fluoride ions—contained smaller particles with both spherical and straight facets. The BV-III sample contained even smaller spherical particles; BV-IV contained huge aggregates of very small particles, and lastly, BV-V could be described with thin, compressed, “comb-like” morphology.

The optical properties were investigated by UV–Vis DR spectroscopy (Figure 7). From the DR spectra, the band gap values (Figure 7) were also calculated using the Kubelka–Munk equation. The band gap values were between 2.30 and 2.38 eV, which indicates that these photocatalysts can be excited with visible light up to 520–539 nm wavelengths.

Photocatalytic activities of the synthesized  $\text{BiVO}_4$  photocatalysts were compared with each other and also with commercial Aeroxide P25  $\text{TiO}_2$  (Figure 8). Before the photocatalytic decomposition, the suspensions were kept in the dark to reach adsorption–desorption equilibrium. Most of the nanomaterials adsorbed 3%–5% of methylene blue, except BV-IV, which adsorbed 35%. The  $\text{TiO}_2$  had negligible photocatalytic efficiency under visible light irradiation: the concentration of methylene blue decreased the same way as in the case of simple photolysis (i.e., visible light irradiation, without any nanomaterial). All the synthesized  $\text{BiVO}_4$  photocatalysts showed great photocatalytic activity; however, in the case of BV-I and BV-II samples, it was slightly lower (88% and 85% decomposition after 60 min of irradiation, respectively)

compared with the BV-III, BV-IV, and BV-V photocatalysts because these nanomaterials decomposed more than 90% of the dye molecules in the first 40 min of the irradiation. So both the intense fluorination of the surface (BV-III) and the synthesis of porous  $\text{BiVO}_4$  photocatalysts (BV-IV) proved to be efficient to achieve excellent photocatalytic activity, whose results are in good accordance with the literature.<sup>59,60</sup> It should be mentioned that in the case of BV-IV, the enhanced adsorption capacity could also contribute to the high photocatalytic activity.

### 3.2 | Photocatalytic activities of $\text{TiO}_2/\text{WO}_3$ composite-covered membranes

As detailed in Section 2.3, 2.5, 5, 10, and 25 wt%  $\text{WO}_3$  containing  $\text{TiO}_2/\text{WO}_3$  composite-covered membranes were prepared, and their photocatalytic activities were also investigated by using the modified Millipore membrane photoreactor (Figure 3). Both visible and UV light irradiations were investigated, and the concentration decreases—after 120 min of irradiation—were compared with the pure (100%)  $\text{TiO}_2$ -covered membrane (Figure 9). A slight photocatalytic enhancement was achieved in the case of 5 wt% of  $\text{WO}_3$  content. Higher and lower  $\text{WO}_3$  contents did not increase the photocatalytic efficiency significantly.

### 3.3 | Effects of $\text{TiO}_2$ , $\text{BiVO}_4$ , and $\text{WO}_3$ coatings on the membrane filtration of oil-in-water emulsions

In the next experimental series, the effects of the pure  $\text{TiO}_2$ , five different  $\text{BiVO}_4$ , and  $\text{WO}_3$  coatings on the membrane



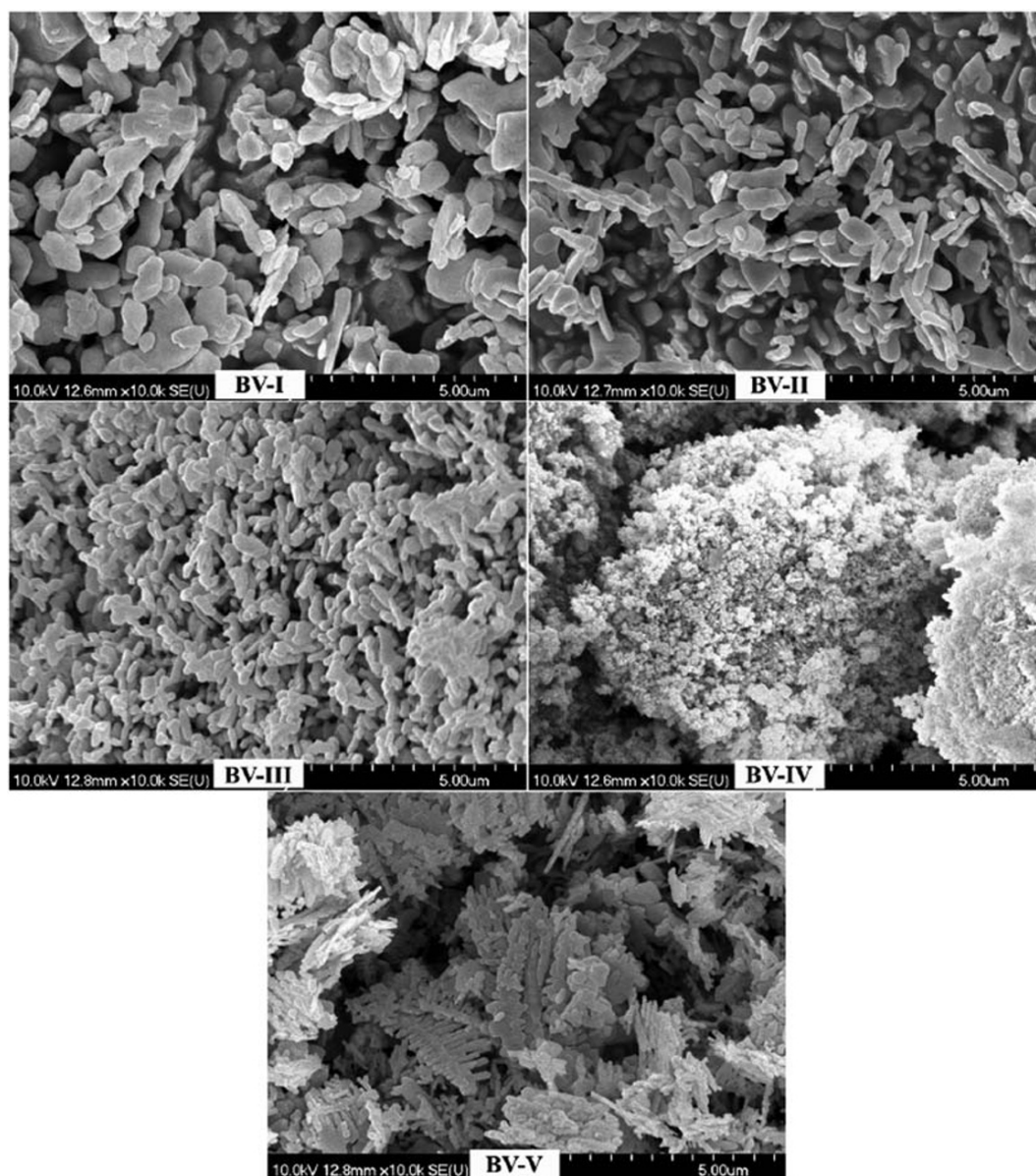


**FIGURE 6** Scanning electron microscopy (SEM) micrographs of BV-I–V bismuth vanadate photocatalysts

filtration efficiency of o/w emulsions ( $100 \text{ mg L}^{-1}$  crude oil content) were investigated. All of the filtration experiments were carried out in three steps: first, the flux of distilled water was determined, then the flux was continuously followed during the filtration of the o/w emulsion until the VRR reached 5, and finally, the water flux was remeasured after rinsing the membrane. On the basis of the measured fluxes (Figure 10), the filtration resistances (Figure 11) were calculated as detailed in Section 2.6.1.

In the case of the uncoated membrane, the flux intensively decreased at the very beginning of the filtration (Figure 10) because of the early formation of a hydrophobic cake layer, which was built up by the attached oil droplets. At the end of the filtration, only  $87 \text{ L m}^{-2} \text{ h}^{-1}$  flux was measured. Therefore, the calculated total

resistance was very high (Figure 11), which was caused mainly by the irreversible resistance, but the reversible resistance was also significant. This means that the fouling, the strong attachment of the droplets, and the concentration polarization also contributed to the intense flux reduction. Coating with  $\text{TiO}_2$  resulted in significantly higher (almost doubled:  $155 \text{ L m}^{-2} \text{ h}^{-1}$ ) flux (Figure 10) and a considerable reduction of both irreversible and reversible resistances (Figure 11). The reduced fouling and reduced attachment of the oil droplets resulted in a significant reduction of the total filtration resistance due to the  $\text{TiO}_2$  coating.

All the  $\text{BiVO}_4$  photocatalyst coatings significantly reduced the irreversible resistance (Figure 11). BV-I coating resulted in the best filtration properties: the flux was



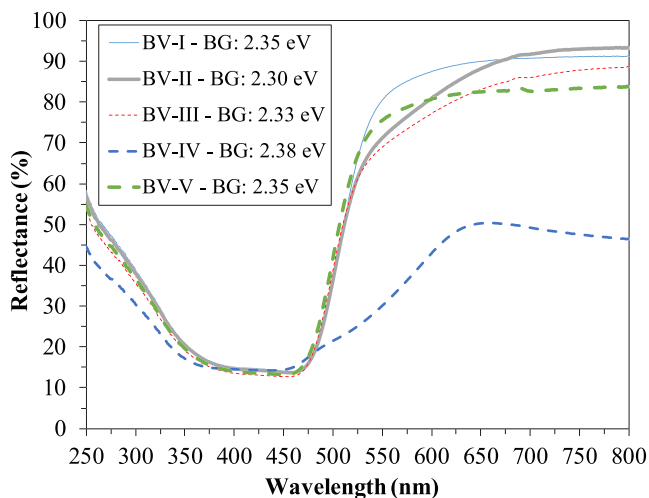


**FIGURE 7** Diffuse reflectance (DR) spectra of the synthesized BiVO<sub>4</sub> photocatalysts and the calculated band gap values (by using the Kubelka-Munk equation for the calculations)

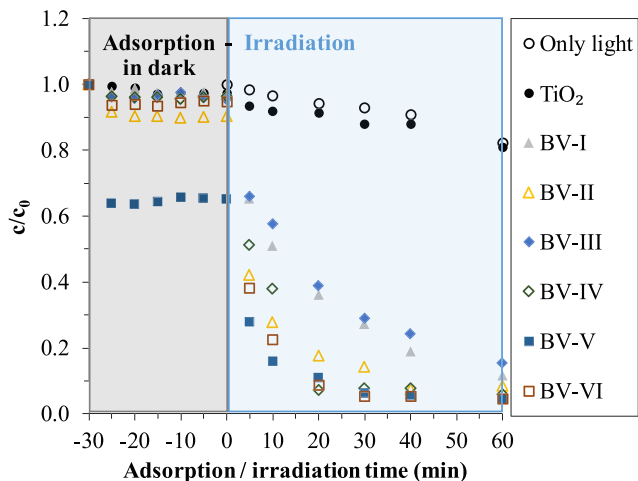


**FIGURE 8** Photocatalytic activity experiments using the BiVO<sub>4</sub> photocatalysts in suspension form, under visible light irradiation

464 L m<sup>-2</sup> h<sup>-1</sup>, and negligible reversible and irreversible resistances were measured, which resulted in by far the lowest total filtration resistance value of the series. Despite the relatively low photocatalytic activity of this photocatalyst compared with most of the other BiVO<sub>4</sub> samples, only this material can be beneficial for membrane surface modification, because of the following results.

The BV-II and BV-III photocatalysts also resulted in very low irreversible resistances, but because of the significant reversible resistances, the measured fluxes (86 and 128 L m<sup>-2</sup> h<sup>-1</sup>, respectively) were lower, compared with the fluxes provided by the TiO<sub>2</sub> or BV-I coatings (155 and 464 L m<sup>-2</sup> h<sup>-1</sup>, respectively). These results can be related to the fluorinated surfaces of these

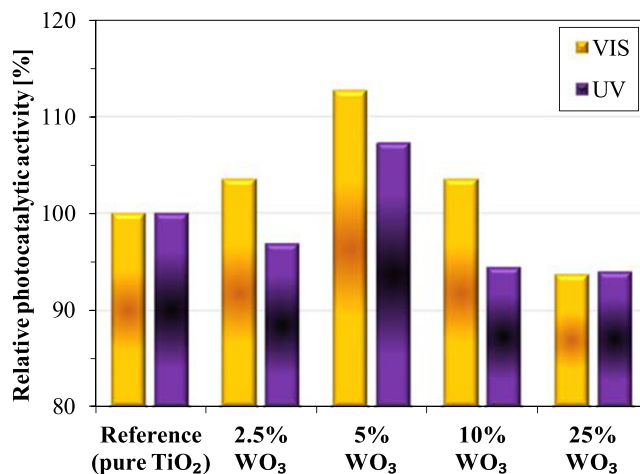


**FIGURE 9** Relative photocatalytic activities of different TiO<sub>2</sub>/WO<sub>3</sub> composite-covered membranes compared with the activity of pure TiO<sub>2</sub>-covered membrane

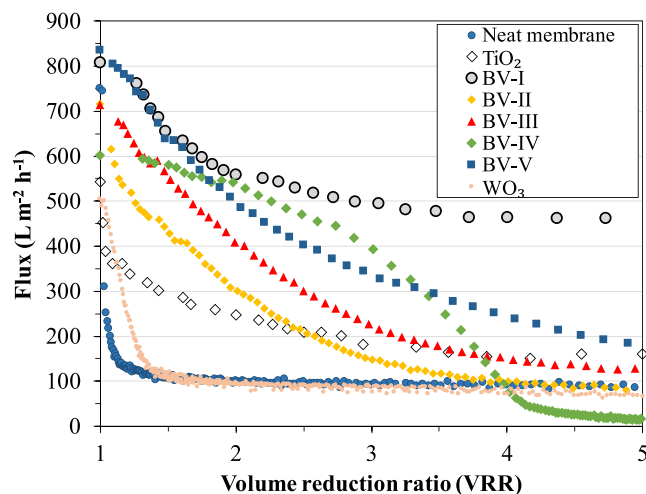


**FIGURE 10** Representative flux curves, measured during the filtration of the o/w emulsions with the different membranes until the volume reduction ratio (VRR) was 5

nanomaterials, which resulted in increased photocatalytic activity, as it was expected.<sup>59</sup> However, fluorination of the surface can result in less hydrophilic properties (higher water contact angles)—as it has already been proven for TiO<sub>2</sub> nanomaterials<sup>63</sup>—which slightly facilitates the adherence of the hydrophobic oil droplets.

In the case of the BV-IV coating, the measured zero irreversible resistance was caused only by an apparent total flux recovery: during the cleaning procedure of the membrane—after using it for o/w emulsion separation—not only the contaminant layer but also the BV-IV particles were removed from the membrane surface. In addition to the fact that during the filtration, the flux was significantly reduced—to 14 L m<sup>-2</sup> h<sup>-1</sup> at the end of the

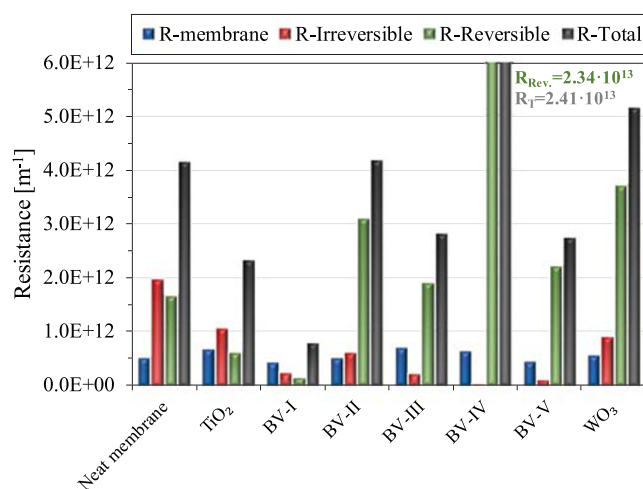


**FIGURE 11** Different filtration resistances during the filtration of  $100 \text{ mg L}^{-1}$  o/w emulsion, in the case of the neat and the different nanomaterial-coated membranes

experiment—it can be also stated that this porous  $\text{BiVO}_4$  with high adsorption capacity cannot be recommended for membrane surface modification, because even at the beginning of the filtration, relatively high fluxes were measured, but at higher VRR values, the flux was reduced significantly (Figure 10). The BV-V coating reduced the total filtration resistance, compared with the neat membrane, but slight particle leaching was observed in this case as well.

The  $\text{WO}_3$  coating was not beneficial either concerning the filtration of o/w emulsion, because a relatively low flux ( $70 \text{ L m}^{-2} \text{ h}^{-1}$ ) was measured (Figure 10) and a high total filtration resistance was calculated (Figure 11). Nevertheless, because the 5 wt%  $\text{WO}_3$  content in the  $\text{TiO}_2/\text{WO}_3$  composites was beneficial concerning the photocatalytic activity, the investigation of the composites containing 5 wt%  $\text{WO}_3$  was also carried out in the following experiment series.

On the basis of the extractable oil content and COD of the permeates, higher than 97% purification efficiencies can be achieved with the used PVDF membranes, and no significant differences were observed in relation to the absence or presence of the different nanomaterial coatings.

### 3.4 | Solar photocatalytic recovery of the different nanomaterial-coated membranes

In the next experimental series, various nanomaterial-covered membranes were used for the filtration of o/w emulsions, and then solar photocatalytic purification of the contaminated surfaces was carried out. For these experiments, a neat membrane (as control), a  $\text{TiO}_2$ -

coated membrane, a BV-I-coated membrane (as the most beneficial  $\text{BiVO}_4$ , in relation to the filtration properties), a  $\text{WO}_3$ -coated membrane (as control), and four different  $\text{TiO}_2/\text{BiVO}_4/(\text{WO}_3)$  composite-coated membranes were used (compositions are detailed in Table 1). The filtration resistances (Figure 12), FRR (Table 1), and FDR (Table 1) were also calculated (as it is detailed in Section 2.6.1). A number was assigned to the different nanomaterial-coated membranes, as detailed in Table 1.

First, the results of the filtration experiments before the solar regeneration are discussed. On the basis of the filtration resistances—taking the results of membranes 1–4 into account, which were discussed in the previous section—it can be stated that 5 and 20 wt% BV-I containing  $\text{TiO}_2/\text{BiVO}_4$  composites (membranes 5 and 6; respectively) provided better conditions than the pure  $\text{TiO}_2$  coating, as total filtration resistances and irreversible resistances were lower, but these coatings were not as beneficial as the pure BV-I coating (Figure 12). Regarding the total filtration resistance, the 5 wt%  $\text{WO}_3$  containing  $\text{TiO}_2/\text{BiVO}_4/\text{WO}_3$  composite coatings (membranes 7 and 8, with 5 wt% and 20 wt% BV-I contents, respectively) were also more beneficial than simple  $\text{TiO}_2$  coating, but in these cases, the irreversible resistances were higher. Consequently, the application of  $\text{WO}_3$  as a composite component of membrane coatings is not recommended.

Because higher FRR values indicate more effective flux recovery—reached by water rinsing—pure BV-I (membrane 3) and 20 wt% BV-I containing  $\text{TiO}_2/\text{BiVO}_4$  composite (membrane 6) coatings resulted in the best cleanability, as 66% and 52% FRR values were calculated, respectively (Table 1). Moreover, simple BV-I coating (membrane 3) was the most beneficial in relation with

**TABLE 1** Membrane nanomaterial coating compositions, FRR, and FDR values of the different membranes

No.	Membrane	FRR (%)	FDR (%)
1	Neat commercial PVDF	22	87
2	PVDF + $\text{TiO}_2$	33	75
3	PVDF + $\text{BiVO}_4$	66	45
4	PVDF + $\text{WO}_3$	40	89
5	PVDF + $\text{TiO}_2(95\%)/\text{BiVO}_4(5\%)$	45	71
6	PVDF + $\text{TiO}_2(80\%)/\text{BiVO}_4(20\%)$	52	70
7	PVDF + $\text{TiO}_2(90\%)/\text{BiVO}_4(5\%)/\text{WO}_3(5\%)$	31	73
8	PVDF + $\text{TiO}_2(75\%)/\text{BiVO}_4(20\%)/\text{WO}_3(5\%)$	40	72

Abbreviations: FDR, flux decay ratio; FRR, flux recovery ratio; PVDF, polyvinylidene fluoride.

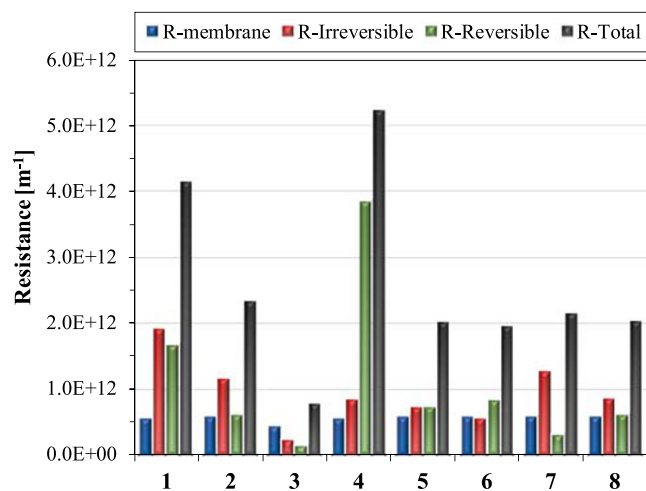


**FIGURE 12** Different filtration resistances during the filtration of  $100 \text{ mg L}^{-1}$  o/w emulsion, in the case of the neat, different nanomaterial-, and different nanocomposite-coated membranes (coating compositions are defined in Table 1)

the FDR values (45%) as well, because the lower FDR values indicate lower fouling and lower flux reduction during the filtration. All the other BV-I containing composite coatings (membranes 5–8) also resulted in better FDR values (70%–73%) than the neat (FDR = 87%),  $\text{TiO}_2$ -coated (FDR = 75%), or  $\text{WO}_3$ -coated (FDR = 89%) membranes, which proves the general advantage of the presence of this material on the membrane surface, in the case of o/w emulsion separation.

After the filtration of the emulsion, followed by intensive rinsing, the water fluxes were measured again (to calculate the FRR values), and then the photocatalytic purification of the membrane surfaces were carried out by solar irradiation as it is detailed in Section 2.7. The water fluxes were measured again after 150 min of irradiation to characterize the photocatalytic flux recovery, named as “Solar-FRR” (Figure 13).

The lowest (22%) FRR value was determined for the neat membrane, and slightly enhanced relative flux (26%) was measured after the 150 min solar irradiation (Solar-FRR). This indicates that the contaminant layer cannot be eliminated by the applied stirring, nor can it be decomposed by photolysis with the UV photons of the solar irradiation.

On the basis of Figure 13, it may look like that the pure  $\text{WO}_3$  coating ensured 100% flux recovery, but it was again only an apparent recovery because it was caused by the significant leaching of the  $\text{WO}_3$  nanoparticles together with the contaminants. Moreover, the immobilization of other  $\text{WO}_3$  containing nanocomposites (membranes 7 and 8) were also not long-lasting.

As the higher FRR values are beneficial, the membrane 3 and membrane 6 were the most beneficial both

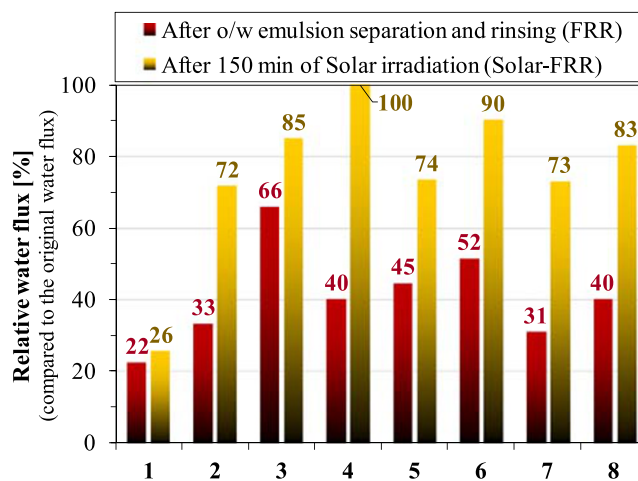


**FIGURE 13** Solar photocatalytic flux recoveries after 150 min of solar irradiation of the contaminated membranes (coating compositions are defined in Table 1)

before (FRR) and after solar irradiation (Solar-FRR). Among them, the pure BV-I coating (membrane 3) had higher FRR value but lower Solar-FRR value, whereas the 20 wt% BV-I containing  $\text{TiO}_2/\text{BiVO}_4$  composite coating (membrane 6) had lower FRR but higher Solar-FRR value, which indicates much higher solar photocatalytic activity for the  $\text{TiO}_2$  containing coating. This result is in good accordance with the fact that the most significant differences between FRR and Solar-FRR values were determined in the case of the pure  $\text{TiO}_2$  coating (Solar-FRR was 2.2 times higher than FRR in this case), which clearly indicates that  $\text{TiO}_2$  is more effective in decomposing oily contaminants than the BV-I photocatalyst under solar irradiation.

In summary, pure BV-I coating was the most beneficial in relation with the filtration properties, whereas pure  $\text{TiO}_2$  coating was the most beneficial concerning the photocatalytic purification of the contaminated membrane, and the  $\text{TiO}_2(80\%)/\text{BiVO}_4(20\%)$  composite represented a good compromise, as it resulted in the second highest FRR and the highest Solar-FRR value.

Additionally, for the interpretation of the high solar photocatalytic recovery efficiency of the  $\text{TiO}_2$  coating, the photocatalytic efficiency of the pure  $\text{TiO}_2$  and BV-I-coated membranes were compared in the modified PMR. The results proved that when UV photons are used for the excitation of the photocatalysts, the  $\text{TiO}_2$  showed significantly (almost twice) higher efficiency.

### 3.5 | Discussion

Similarly to other studies, the  $\text{TiO}_2$  coating resulted in significant flux enhancement and reduced membrane

fouling. In the present study, the used commercial neat PVDF membrane provided only  $87 \text{ L m}^{-2} \text{ h}^{-1}$  flux, which was increased by 78%, achieving  $155 \text{ L m}^{-2} \text{ h}^{-1}$  flux in the case of the used 0.1 MPa transmembrane pressure during the filtration of  $100 \text{ mg L}^{-1}$  o/w emulsion. In comparison, Ong et al.<sup>49</sup> measured only  $32.5 \text{ L m}^{-2} \text{ h}^{-1}$  flux for a neat PVDF membrane (with  $0.1 \mu\text{m}$  pore size) during the filtration of a  $250 \text{ mg L}^{-1}$  o/w emulsion which was increased up to only  $75.7 \text{ L m}^{-2} \text{ h}^{-1}$  with  $\text{TiO}_2$  modification, and the authors did not investigate the photocatalytic purification of the used membranes. Moslehyani et al.<sup>34</sup> also modified PVDF membranes ( $d_{\text{pore}} = 50 \text{ nm}$ ) with  $\text{TiO}_2$ , achieving close to twice as high fluxes during the filtration of  $200 \text{ mg L}^{-1}$  oil in water emulsion at different (0.02–0.08 MPa) transmembrane pressures. The highest flux was  $95 \text{ L m}^{-2} \text{ h}^{-1}$ , which was achieved by setting a 0.08-MPa pressure. The authors also proved the successful photocatalytic decomposition of the filtered oil contaminants, as GC–MS peaks of the retentate were reduced by more than 90% after 8 h of UV irradiation, and the hydrocarbon concentration of the permeate was found to be below the EU standards, similar to our results. Significant flux ( $382 \text{ L m}^{-2} \text{ h}^{-1}$ ) was also achieved by Shi et al.<sup>35</sup>—by modifying a PVDF membrane with  $\text{TiO}_2$ —during the filtration of a diesel/water emulsion, applying 0.09 MPa transmembrane pressure. To the best of our knowledge, there is no publication in the literature about the preparation of  $\text{BiVO}_4$  photocatalyst-modified membranes and their application for o/w emulsion separation. The presented (i) high flux ( $464 \text{ L m}^{-2} \text{ h}^{-1}$ ) which exceeded all the mentioned results, (ii) the estimated low FDR (FDR = 45%) and (iii) the high FRR (FRR = 66%) in the case of pure  $\text{BiVO}_4$  (BV-I) coating, and finally, (iv) the effective solar photocatalytic recovery—especially in the case of the  $\text{TiO}_2(80\%)/\text{BiVO}_4(20\%)$  composite—indicate that  $\text{BiVO}_4$  photocatalysts and their composites deserve attention in the research area of nanocomposite-based photocatalytic membranes and that they are worth applying for oil-in-water emulsion separation. Investigation of other immobilization methods—like blending or chemical immobilization—is also highly recommended as during long-term application, these methods are more beneficial to preparing composite membranes.<sup>44</sup> Although  $\text{WO}_3$  did not live up to our expectations in the present study, the investigation of three-component composites is recommended as they are promising in achieving low band gap and suppressed recombination ratio at the same time. For example, graphene oxides and CNTs are also promising for use as the third component of a  $\text{TiO}_2/\text{BiVO}_4$  or other composite systems, as they can improve the homogeneity and/or the antifouling properties of the surfaces and may also suppress the charge carrier recombination.<sup>38,45,47</sup>

## 4 | CONCLUSIONS

$\text{WO}_3$  was found to be inappropriate for membrane surface modification with physical deposition, as it resulted in low flux ( $70 \text{ L m}^{-2} \text{ h}^{-1}$ ) and high total filtration resistance; moreover, during the solar photocatalytic regeneration of the  $\text{WO}_3$ -coated membrane, significant leaching of the nanoparticles was observed. Furthermore, despite the slight positive effect of the presence of 5 wt%  $\text{WO}_3$  in nanocomposites, the immobilization of these composites were not long-lasting.

$\text{TiO}_2$ ,  $\text{BiVO}_4$ , and their composites can also be used to modify membrane surfaces used in o/w emulsion separation. Pure  $\text{BiVO}_4$  coating was more beneficial concerning the filtration properties, whereas pure  $\text{TiO}_2$  coating was more beneficial in relation to the photocatalytic purification of the fouled membrane. The  $\text{TiO}_2(80\%)/\text{BiVO}_4(20\%)$  composite represented a good compromise that could be purified with solar irradiation with high efficiency without the application of any purifying chemical. On the basis of the presented results,  $\text{BiVO}_4$  photocatalysts are promising for a more thorough investigation for the preparation of nanomaterial-modified photocatalytic membranes.

Nanocomposite-based photocatalytic membranes are very promising for the treatment of oil-contaminated waters, because they combine advanced antifouling and self-cleaning properties; thus, this field is thoroughly investigated, and after pilot-scale studies, industrial applications are also expected in the near future.

## ACKNOWLEDGEMENTS

This project was supported by the Hungarian Science and Research Foundation (2017-2.3.7-TÉT-IN-2017-00016), by the Hungarian State and the European Union (EFOP-3.6.2-16-2017-00010), and by the Ministry of Science and Technology of the Government of India (DST/INT/HUN/P17/2017). Erika Nascimben Santos is grateful for the financial support of the Stipendium Hungaricum scholarship. Gábor Veréb is grateful for the financial the support of the János Bolyai Research Scholarship of the Hungarian Academy of Sciences. Open access funding was provided by the University of Szeged (SZTE, Grant Number: 4541). The authors are grateful to Tamás Gyulavári for his valuable contribution in proof-reading the manuscript.

## ORCID

Erika Nascimben Santos  <https://orcid.org/0000-0002-6273-2923>


Szabolcs Kertész  <https://orcid.org/0000-0001-9760-3008>

Zsolt Pap  <https://orcid.org/0000-0002-8049-0809>

Zsolt Kása  <https://orcid.org/0000-0003-4352-7761>

Tünde Alapi  <https://orcid.org/0000-0002-9869-9280>



Gangasalam Arthanareeswaran  <https://orcid.org/0000-0002-6166-8018>

Klara Hernadi  <https://orcid.org/0000-0001-9419-689X>

Gábor Veréb  <https://orcid.org/0000-0001-9642-1851>

## REFERENCES

- Padaki M, Surya Murali R, Abdullah MS, et al. Membrane technology enhancement in oil–water separation. A Review. *Desalination*. 2015;357:197-207.
- Chaturvedi KR, Singh AK, Sharma T. Impact of shale on properties and oil recovery potential of sandstone formation for low-salinity waterflooding applications. *Asia-Pacific J Chem Eng*. 2019;14(5):1–14, e2352. <https://doi.org/10.1002/apj.2352>
- Currie G. Lies, damned lies, AVs, shared mobility, and urban transit futures. *J Public Transp*. 2018;21(1):19-30.
- Zhao M, Yang D, Feng S, Liu H. Vanpool trip planning based on evolutionary multiple objective optimization. *IOP Conf Ser Earth Environ Sci*. 2017;81:1–16, 012206. <https://doi.org/10.1088/1755-1315/81/1/012206>
- Boleydei H, Mirghaffari N, Farhadian O. Comparative study on adsorption of crude oil and spent engine oil from seawater and freshwater using algal biomass. *Environ Sci Pollut Res Int*. 2018; 25(21):21024-21035.
- Yang R, Zhang G, Li S, et al. Degradation of crude oil by mixed cultures of bacteria isolated from the Qinghai-Tibet plateau and comparative analysis of metabolic mechanisms. *Environ Sci Pollut Res Int*. 2019;26(2):1834-1847.
- Li C, Fu L, Stafford J, Belosevic M, Gamal E-DM. The toxicity of oil sands process-affected water (OSPW): a critical review. *Sci Total Environ*. 1785-1802;2017:601-602.
- Côté RP. The effects of petroleum refinery liquid wastes on aquatic life: with special emphasis on the Canadian environment. National Research Council of Canada, NRC Associate Committee on Scientific Criteria for Environmental Quality; 1976.
- Wake H. Oil refineries: a review of their ecological impacts on the aquatic environment. *Estuar Coast Shelf Sci*. 2005;62(1–2): 131-140.
- Tang J, Wang M, Wang F, Sun Q, Zhou Q. Eco-toxicity of petroleum hydrocarbon contaminated soil. *J Environ Sci*. 2011; 23(5):845-851.
- Ramadass K, Megharaj M, Venkateswarlu K, Naidu R. Ecological implications of motor oil pollution: earthworm survival and soil health. *Soil Biol Biochem*. 2015;85:72-81.
- Iqbal M, Nisar J, Adil M, et al. Mutagenicity and cytotoxicity evaluation of photo-catalytically treated petroleum refinery wastewater using an array of bioassays. *Chemosphere*. 2017; 168:590-598.
- Abdel-Shafy HI, Mansour MSM. A review on polycyclic aromatic hydrocarbons: source, environmental impact, effect on human health and remediation. *Egyptian J Petrol*. 2016;25(1): 107-123.
- Tasker TL, Burgos WD, Piotrowski P, et al. Environmental and human health impacts of spreading oil and gas wastewater on roads. *Environ Sci Technol*. 2018;52(12):7081-7091.
- Cai Y, Chen D, Li N, et al. A smart membrane with antifouling capability and switchable oil wettability for high-efficiency oil/water emulsions separation. *J Membr Sci*. 2018;555:69-77.
- Wu J, Wei W, Li S, et al. The effect of membrane surface charges on demulsification and fouling resistance during emulsion separation. *J Membr Sci*. 2018;563:126-133.
- Stewart M, Arnold K. Produced water treating systems. In: *Emulsions and Oil Treating Equipment*. Burlington, MA, USA: Gulf Professional Publishing; 2009:107-211.
- Hong PK, Xiao T. Treatment of oil spill water by ozonation and sand filtration. *Chemosphere*. 2013;91(5):641-647.
- Cambiella A, Benito JM, Pazos C, Coca J. Centrifugal separation efficiency in the treatment of waste emulsified oils. *Chem Eng Res Des*. 2006;84(1):69-76.
- Maruyama H, Tada Y, Seki H. Enhancement of oil droplet removal from o/w emulsion by adding methylated milk casein in flotation technique. *Asia-Pacific J Chem Eng*. 2009;4(2): 211-217.
- Zolfaghari R, Fakhru'l-Razi A, Abdullah LC, Elnashaie SSEH, Pendashteh A. Demulsification techniques of water-in-oil and oil-in-water emulsions in petroleum industry. *Sep Purif Technol*. 2016;170:377-407.
- Veréb G, Nagy L, Kertész S, Kovács I, Hodúr C, László Z. Highly efficient purification of finely dispersed oil contaminated waters by coagulation/flocculation method and effects on membrane filtration. *Studia UBB Chemia*. 2017;62(2): 259-270.
- Zhang Q, Liu N, Cao Y, et al. A facile method to prepare dual-functional membrane for efficient oil removal and in situ reversible mercury ions adsorption from wastewater. *Appl Surf Sci*. 2018;434:57-62.
- Saki S, Uzal N. Preparation and characterization of PSF/PEI/CaCO<sub>3</sub> nanocomposite membranes for oil/water separation. *Environ Sci Pollut Res Int*. 2018;25(25):25315-25326.
- Zhao D, Su C, Liu G, Zhu Y, Gu Z. Performance and autopsy of nanofiltration membranes at an oil-field wastewater desalination plant. *Environ Sci Pollut Res Int*. 2019;26(3): 2681-2690.
- Golpour M, Pakizeh M. Development of a new nanofiltration membrane for removal of kinetic hydrate inhibitor from water. *Sep Purif Technol*. 2017;183:237-248.
- Zhu Y, Wang D, Jiang L, Jin J. Recent progress in developing advanced membranes for emulsified oil/water separation. *NPG Asia Materials*. 2014;6(5):e101-e101.
- Van der Bruggen B. Chemical modification of polyethersulfone nanofiltration membranes: a review. *J Appl Polym Sci*. 2009; 114(1):630-642.
- Rana D, Matsuura T. Surface modifications for antifouling membranes. *Chem Rev*. 2010;110(4):2448-2471.
- Karimnezhad H, Rajabi L, Salehi E, Derakhshan AA, Azimi S. Novel nanocomposite Kevlar fabric membranes: fabrication characterization, and performance in oil/water separation. *Appl Surf Sci*. 2014;293:275-286.
- Mofakhami Mehrabadi M, Aghaei A, Sahba Yaghmaee M, Karimnezhad M, Kamari M. The effect of functional carbon nanotubes on the permeability of ultrafiltration nanocomposite PVDF membranes. *Asia-Pacific J Chem Eng*. 2018;13(2): e2180.1–11. <https://doi.org/10.1002/apj.2180>
- Anwar F, Arthanareeswaran G. Silver nano-particle coated hydroxyapatite nano-composite membrane for the treatment of palm oil mill effluent. *J Water Process Eng*. 2019;31:100844. <https://doi.org/10.1016/j.jwpe.2019.100844>

33. Chang Q, Zhou J-E, Wang Y, et al. Application of ceramic microfiltration membrane modified by nano-TiO<sub>2</sub> coating in separation of a stable oil-in-water emulsion. *J Membr Sci.* 2014; 456:128-133.
34. Moslehyani A, Ismail AF, Othman MHD, Matsuura T. Hydrocarbon degradation and separation of bilge water via a novel TiO<sub>2</sub>-HNTs/PVDF-based photocatalytic membrane reactor (PMR). *RSC Adv.* 2015;5(19):14147-14155.
35. Shi H, He Y, Pan Y, et al. A modified mussel-inspired method to fabricate TiO<sub>2</sub> decorated superhydrophilic PVDF membrane for oil/water separation. *J Membr Sci.* 2016;506:60-70.
36. Tan BYL, Tai MH, Juay J, Liu Z, Sun D. A study on the performance of self-cleaning oil-water separation membrane formed by various TiO<sub>2</sub> nanostructures. *Sep Purif Technol.* 2015;156: 942-951.
37. Kovács I, Veréb G, Kertész S, Hodúr C, László Z. Fouling mitigation and cleanability of TiO<sub>2</sub> photocatalyst-modified PVDF membranes during ultrafiltration of model oily wastewater with different salt contents. *Environ Sci Pollut Res.* 2018;25(35): 34912-34921.
38. Veréb G, Kálmán V, Gyulavári T, et al. Advantages of TiO<sub>2</sub>/carbon nanotube modified photocatalytic membranes in the purification of oil-in-water emulsions. *Water Sci Technol Water Supply.* 2018;19(4):1167-1174.
39. Venkatesh K, Arthanareeswaran G, Bose AC. PVDF mixed matrix nano-filtration membranes integrated with 1D-PANI/TiO<sub>2</sub> NFs for oil-water emulsion separation. *RSC Adv.* 2016;6 (23):18899-18908.
40. Mozia S. Photocatalytic membrane reactors (PMRs) in water and wastewater treatment. A Review. *Sep Purif Technol.* 2010; 73(2):71-91.
41. Loddo V, Augugliaro V, Palmisano L. Photocatalytic membrane reactors: case studies and perspectives. *Asia-Pacific J Chem Eng.* 2009;4(3):380-384.
42. Veréb G, Ambrus Z, Pap Z, Mogyorosi K, Dombi A, Hernadi K. Immobilization of crystallized photocatalysts on ceramic paper by titanium (IV) ethoxide and photocatalytic decomposition of phenol. *React Kinet Mech Catal.* 2014;113(1):293-303.
43. Argurio P, Fontananova E, Molinari R, Drioli E. Photocatalytic membranes in photocatalytic membrane reactors. *Processes.* 2018;6(9):162. <https://doi.org/10.3390/pr6090162>
44. Nascimbén Santos É, László Z, Hodúr C, Arthanareeswaran G, Veréb G. Photocatalytic membrane filtration and its advantages over conventional approaches in the treatment of oily wastewater: a review. *Asia-Pacific J Chem Eng.* 2020. <https://doi.org/10.1002/apj.2533>
45. Veréb G, Kassai P, Nascimben Santos E, Arthanareeswaran G, Hodur C, Laszlo Z. Intensification of the ultrafiltration of real oil-contaminated (produced) water with pre-ozonation and/or with TiO<sub>2</sub>, TiO<sub>2</sub>/CNT nanomaterial-coated membrane surfaces. *Environ Sci Pollut Res Int.* 2020;27(18):22195-22205.
46. Chen Q, Yu Z, Li F, et al. A novel photocatalytic membrane decorated with RGO-Ag-TiO<sub>2</sub> for dye degradation and oil-water emulsion separation. *J Chem Technol Biotechnol.* 2017;93 (3):761-775.
47. Venkatesh K, Arthanareeswaran G, Bose AC, Kumar PS. Hydrophilic hierarchical carbon with TiO<sub>2</sub> nanofiber membrane for high separation efficiency of dye and oil-water emulsion. *Sep Purif Technol.* 2020;241:116709. <https://doi.org/10.1016/j.seppur.2020.116709>
48. Wang B, Chen C, Liu H, Xia B, Fan Y, Chen T. WO<sub>3</sub>/TiO<sub>2</sub> superhydrophilic and underwater superoleophobic membrane for effective separation of oil-in-water emulsions. *Thin Solid Films.* 2018;665:9-16.
49. Ong CS, Lau WJ, Goh PS, Ng BC, Ismail AF. Preparation and characterization of PVDF-PVP-TiO<sub>2</sub> composite hollow fiber membranes for oily wastewater treatment using submerged membrane system. *Desalin Water Treat.* 2015;53(5): 1213-1223.
50. Iwase M, Yamada K, Kurisaki T, Prieto-Mahaney OO, Ohtani B, Wakita H. Visible-light photocatalysis with phosphorus-doped titanium (IV) oxide particles prepared using a phosphide compound. *Appl Catal B.* 2013;132-133: 39-44.
51. Réti B, Mogyorósi K, Dombi A, Hernádi K. Substrate dependent photocatalytic performance of TiO<sub>2</sub>/MWCNT photocatalysts. *Appl Catal Gen.* 2014;469:153-158.
52. Bardos E, Kovacs G, Gyulavari T, et al. Novel synthesis approaches for WO<sub>3</sub>-TiO<sub>2</sub>/MWCNT composite photocatalysts-problematic issues of photoactivity enhancement factors. *Catal Today.* 2018;300:28-38.
53. Baia L, Orbán E, Fodor S, et al. Preparation of TiO<sub>2</sub>/WO<sub>3</sub> composite photocatalysts by the adjustment of the semiconductors' surface charge. *Mater Sci Semicond Process.* 2016;42:66-71.
54. Samsudin MFR, Mahmood A, Sufian S. Enhanced photocatalytic degradation of wastewater over RGO-TiO<sub>2</sub>/BiVO<sub>4</sub> photocatalyst under solar light irradiation. *J Mol Liq.* 2018;268: 26-36.
55. Kunduz S, Pozan Soylu GS. Highly active BiVO<sub>4</sub> nanoparticles: the enhanced photocatalytic properties under natural sunlight for removal of phenol from wastewater. *Sep Purif Technol.* 2015;141:221-228.
56. Jiang H, Dai H, Meng X, et al. Hydrothermal fabrication and visible-light-driven photocatalytic properties of bismuth vanadate with multiple morphologies and/or porous structures for Methyl Orange degradation. *J Environ Sci.* 2012;24 (3):449-457.
57. Hou L, Yang L, Li J, Tan J, Yuan C. Efficient sunlight-induced methylene blue removal over one-dimensional mesoporous monoclinic BiVO<sub>4</sub> nanorods. *J Anal Methods Chem.* 2012;2012: 345247. <https://doi.org/10.1155/2012/345247>
58. Song X, Li Y, Wei Z, Ye S, Dionysiou DD. Synthesis of BiVO<sub>4</sub>/P25 composites for the photocatalytic degradation of ethylene under visible light. *Chem Eng J.* 2017;314:443-452.
59. Liu S, Yin K, Ren W, Cheng B, Yu J. Tandem photocatalytic oxidation of Rhodamine B over surface fluorinated bismuth vanadate crystals. *J Mater Chem.* 2012;22(34):17759-17767.
60. Jiang H, Meng X, Dai H, et al. High-performance porous spherical or octapod-like single-crystalline BiVO<sub>4</sub> photocatalysts for the removal of phenol and methylene blue under visible-light illumination. *J Hazard Mater.* 2012;217-218:92-99.
61. Holzwarth U, Gibson N. The Scherrer equation versus the 'Debye-Scherrer equation'. *Nat Nanotechnol.* 2011;6(9): 534-534.

62. Gillespie JB, Lindberg JD, Laude LS. Kubelka-Munk optical coefficients for a barium sulfate white reflectance standard. *Appl Optics*. 1975;14(4):807-809.
63. Chen Y, Chen F, Zhang J. Effect of surface fluorination on the photocatalytic and photo-induced hydrophilic properties of porous TiO<sub>2</sub> films. *Appl Surf Sci*. 2009;255(12):6290-6296.

**How to cite this article:** Nascimben Santos E, Ágoston Á, Kertész S, et al. Investigation of the applicability of TiO<sub>2</sub>, BiVO<sub>4</sub>, and WO<sub>3</sub> nanomaterials for advanced photocatalytic membranes used for oil-in-water emulsion separation. *Asia-Pac J Chem Eng*. 2020;e2549. <https://doi.org/10.1002/apj.2549>